

DOI:10.17586/1023-5086-2018-85-09-37-45

Новый алгоритм для плавающей подвески тонкого главного зеркала диаметром 1,2 метра

© 2018 XIAOLIN DAI, HAO XIAN, JINLONG TANG, XUEJUN ZHANG, YUDONG ZHANG

Для устранения дополнительных внешних усилий, воздействующих на фиксированные опоры крепления больших главных зеркал при их активной коррекции, часто применяется плавающая подвеска. Рассмотрены принцип использования плавающей подвески и алгоритмы распределения приложенных усилий. Предложен новый алгоритм, напрямую использующий изображение корректируемой поверхности зеркала вместо данных о распределении сил на фиксированных опорах для вычисления усилий обратной связи на актуаторах. Моделирование для проверки и сравнения характеристик различных алгоритмов проводится на тонком основном зеркале диаметром 1,2 м. Его результаты показали, что новый алгоритм так же эффективен, как и лучший традиционный алгоритм: он уменьшает остаточное среднеквадратическое отклонение поверхности зеркала до значения менее 3,5 нм. Исследование работоспособности этого алгоритма показало, что он более чувствителен к отклонению положения фиксированных точек и ошибкам датчика Шека–Гартмана, чем алгоритм, основанный на измерении усилий на опорах, а поскольку предложенный алгоритм не нуждается в датчиках усилий обратной связи, он более пригоден для упрощения конструкции плавающей подвески.

Ключевые слова: адаптивная оптика, тонкое главное зеркало, плавающая подвеска, фиксированные аксиальные точки.

Study on a new floatation support algorithm based on a 1.2 m thin primary mirror

© 2018 г. XIAOLIN DAI^{1, *, **, ***}; HAO XIAN^{**}; JINLONG TANG^{**};
XUEJUN ZHANG^{**}; YUDONG ZHANG^{**}

¹The 38th Research Institute of China Electronics Technology Group Corporation, 199 Xiangzhang Ave. Hefei, China

^{**}Institute of Optics and Electronics, Chinese Academy of Sciences, 1 Xihanggang Ave. Chengdu, China

^{***}University of Chinese Academy of Sciences, Beijing, China

¹E-mail: daixl08@outlook.com

Submitted 14.03.2018

Floatation support is often used to eliminate the extra interaction forces of the large primary mirror's fixed points during the mirror's active correction in order to maintain the mirror's position in the cell. This paper introduces the principle of floatation support as well as its 3 force distribution algorithms. A new floatation support algorithm is proposed, it directly utilizes the image of the mirror surface instead of the fixed points' feedback interaction forces to calculate the adjusting forces of the actuators. Simulations are conducted on a 1.2 m thin primary mirror to verify and compare the performances of all the algorithms, the results show the new algorithm is as effective as the best traditional algorithm – it reduces the residual root mean square of the mirror surface to less than 3.5 nm. Performance study of this new algorithm shows that the new algorithm is more sensitive to the fixed point's position deviation and the Shack-Hartmann's detection error than the force-based-algorithm, but as it doesn't need the force sensors to feedback the interaction forces, it is more helpful to simplify the hardware requirement of floatation support.

Keywords: active optics, thin primary mirror, floatation support, mirror image, axial fixed points.

OCIS codes: 230.4040, 300.6300

1. INTRODUCTION

Active optics is one of the key technologies to build large modern telescopes. By detecting and correcting the mirror surface, active optics can significantly reduce the influence of the mirror's deformations on the beam quality and improve the observation capability of the large telescopes [1, 2].

Least square estimation (LSE) is the most frequently used method to calculate the active correction forces of the actuators on the back of the primary mirrors. However, LSE can't guarantee the resultant force and moments of the actuators to be 0, which means extra pistons and tilts are often introduced to the mirror surface, in other words, the mirror's position in the mirror cell are often changed after regular active correction. Floatation support is usually utilized to solve this problem, by adjusting the active forces of all the actuators according to the feedback extra forces of the fixed points, floatation support can guarantee the extra interaction forces of the fixed points to be 0 thus keeping the mirror at the right position in the cell with minimal effect on the mirror figure. So far, many large telescopes have already implemented active optics and floatation support [3–9]: The Advanced Electro-Optical System telescope and the Discovery Channel Telescope use 3 fixed points, the Starfire Optical Range Telescope and the Multiple Mirror Telescope use 6 fixed points to monitor the positions of the mirror surfaces and implement floatation support. The Very Large Telescope divides its axial support actuators into 3 zones and maintains the primary mirror's position by the 3 virtual fixed points generated by connecting the hydraulic of the actuators in each zone.

This paper firstly introduces the function and influence of the thin mirror's axial fixed points in the mirror's active correction, then introduces the principle of floatation support as well as its 3 force distribution algorithms in section 2. In section 3, we propose a new force distribution algorithm of floatation support which directly utilizes the image of the mirror surface instead of the fixed point's feedback interaction forces to calculate the adjusting forces of the actuators. In section 4, we conduct some simulations on a 1.2 m thin primary mirror to analyze and compare the new algorithm with the traditional algorithms. The results show that the new algorithm is as effective as the best traditional algorithm on correcting the mirror's position with minimal effect on the mirror figure. Performance study of this new algorithm is conducted in section 5, it shows that the new algorithm is more sensitive to the fixed point's position deviation and the Shack-Hartmann's (S-H's) detection error than the force-based-algorithm, but unlike the traditional methods which require both the image of the mirror and the real-time interaction forces of the fixed points, the new method only needs the image of the mirror to conduct

active correction and floatation support, which simplifies its hardware request and makes it easier to achieve.

2. FLOATATION SUPPORT

2.1. Axial fixed points of primary mirror and principle of floatation support

Axial fixed points are used to constrain the axial motion of the primary mirror and are often installed on the back of the mirror. There are usually two kinds of axial fixed points: the first kind doesn't bear any forces [10], while the second kind bears a fraction of the mirror's gravity during normal operation [11, 12]. Figure 1 shows a regular configuration of the axial supports for a 1.2 m thin primary mirror: 36 axial supports distribute as three support rings on the back of the mirror, among them there are 3 axial fixed points and 33 active supports (actuators). For this 1.2 m mirror, all the 36 axial supports bear its axial gravitational loading together, in addition, the 33 active supports can provide active forces during the active correction of the mirror surface.

Usually, axial fixed points don't provide active forces during the active correction, this causes a problem: take the 1.2 m mirror's active correction when the it's mounted vertically as an example, the mirror's surface (W) before the correction is shown

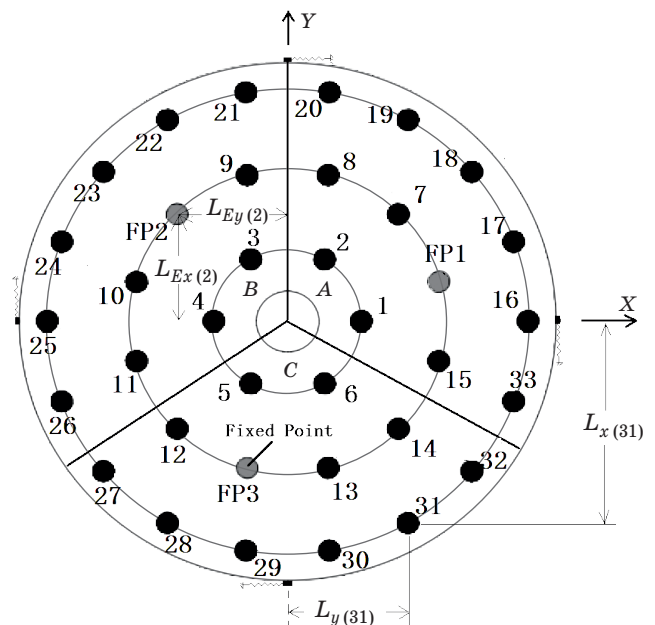


Fig. 1. Configuration of the axial supports for a 1.2 m thin primary mirror. The black and gray spots respectively indicate the actuators and the axial fixed points. $L_{Ex(2)}$ and $L_{Ey(2)}$ are the lengths of the lever arms of the 2nd axial fixed point to the mirror center, $L_{x(31)}$ and $L_{y(31)}$ are the lengths of the lever arms of the 31th active support to the mirror center.

in the Fig. 2a. W is acquired by S-H's sensor with tilt/tip subtracted, this pre-process can reduce the active force range required during the active correction, because the tilt/tip is usually very large amongst all the aberrations and it can be corrected by the secondary mirror. As the 3 axial fixed points are merely passive axial supports, according to the principle of active optics, the active forces of the 33 actuators for correcting W can be calculated by LSE as follows:

$$\mathbf{F} = -(D^T D)^{-1} D^T W, \quad (1)$$

where $\mathbf{F} = [F_1, F_2, \dots, F_{33}]$ are the active forces of the actuators, D is the influence matrix between the actuators and the mirror surface. The mirror surface after applying \mathbf{F} to the actuators is shown in the Fig. 2b, as the 3 axial fixed points can't provide active correction forces, the residual mirror surfaces near these 3 fixed points can't be corrected to 0, thus three "dents" appear on the residual mirror surface at the positions of the fixed points after active correction, which degrades the quality of the active correction. This phenomena can also be explained from another aspect: after the optimization of the axial supports, the normal forces borne by the 1.2 m mirror's axial fixed points should be a permanent fraction of the mirror's axial gravitational loading,

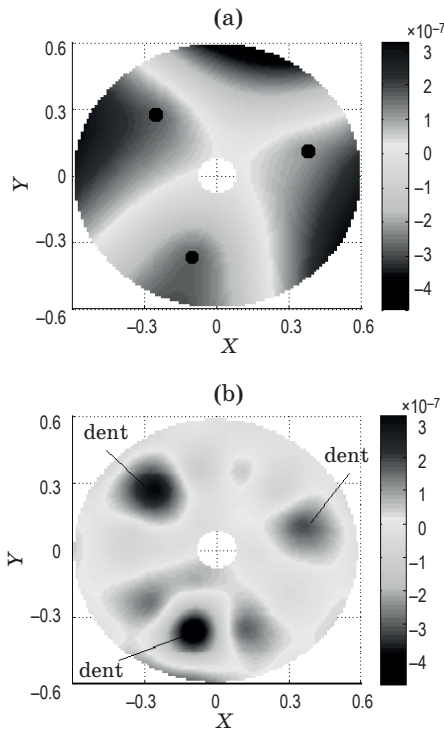


Fig. 2. Mirror surfaces before and after active correction without floatation support. The 3 black dots on the left figure indicate the positions of the 3 axial fixed points. (a) Mirror surface detected by Shack-Hartmann sensor (tilt/tip removed, RMS = 166.4 nm), (b) mirror surface after correction without floatation support (RMS = 41.6 nm).

however, during the active correction, the resultant force and moments of the actuator's correction forces calculated by W with LSE method may not be 0, these resultant force and moments will be borne by the fixed points after the active correction, which leads the fixed points to bear extra interaction forces, thus the "dents" occur.

Floatation support is the mostly frequently used method to solve this problem, its main idea is: by adjusting all the actuators' forces, floatation support generates a reverse resultant force and moment with minimal effect on the mirror surface's shape to compensate those ones borne by the fixed points, in this way, the extra interaction forces borne by the fixed points will be balanced, thus the mirror surface goes back to the ideal position and the "dents" also disappear.

2.2. Force distribution algorithms of floatation support

Usually, balancing the extra resultant force and moments is easy, it is the request introducing minimal deformation on the mirror surface's shape that is the key point of floatation support, this requires an appropriate algorithm to distribute the actuators' forces.

Assume there are n actuators, the force provided by the i^{th} actuator during active correction with floatation support can be written as follows:

$$f_i = G_i \cos\theta + F_i + C_i \quad (i = 1, 2 \dots n), \quad (i = 1, 2, \dots, n) \quad (2)$$

where G_i is the support force of the i^{th} actuator when the mirror is mounted horizontally, θ is the altitude angle of the primary mirror, F_i is the correction force calculated according to the mirror surface acquired by S-H sensor, C_i is the force adjustment during the floatation support. Assume there are m fixed points and the extra interaction force on each fixed point after applying $G_i \cos\theta + F_i$ is E_j , to balance the extra resultant force and moments borne by the fixed points, we have

$$\begin{aligned} \sum_{i=1}^n C_i &= -\sum_{j=1}^m E_j, \\ \sum_{i=1}^n (C_i L_{x(i)}) &= -\sum_{j=1}^m (E_j L_{Ex(j)}), \\ \sum_{i=1}^n (C_i L_{y(i)}) &= -\sum_{j=1}^m (E_j L_{Ey(j)}), \end{aligned} \quad (3)$$

where $L_{Ex(j)}$ and $L_{Ey(j)}$ are the lever arms of the j^{th} axial fixed point to the mirror center, $L_{x(i)}$ and $L_{y(i)}$ are the lever arms of the i^{th} actuator to the mirror center, they have been schematically shown in Fig. 1. Eq. (3) is usually under constraint, which means there are infinite combinations of C_i that can balance

the fixed point's extra resultant force and moments, however, inappropriate combinations may introduce extra deformations to the mirror surface, thus finding an appropriate algorithm of distributing C_i with minimal effect on the mirror figure is vital for the effect of floatation support.

One algorithm distributes C_i uniformly when compensating/balancing the resultant force, as for the resultant moments, it distributes C_i proportionally to the lengths of the actuator's lever arms to the mirror center, thus C_i can be calculated as follows [3, 13]:

Algorithm 1

$$\begin{aligned}
 C_i &= C_{i,F} + C_{i,M_x} + C_{i,M_y} = \\
 &= -\frac{\sum_{j=1}^m E_j}{n} - \sum_{j=1}^m (E_j L_{Ex(j)}) \frac{L_{x(i)}}{\sum_{i=1}^n L_{x(i)}^2} - \\
 &-\sum_{j=1}^m (E_j L_{Ey(j)}) \frac{L_{y(i)}}{\sum_{i=1}^n L_{y(i)}^2} \quad (i = 1, 2, \dots, n),
 \end{aligned} \quad (4)$$

where $C_{i,F}$ is the fraction of C_i used to compensate the fixed point's resultant force, C_{i,M_x} and C_{i,M_y} are the fractions of C_i used to compensate the fixed point's resultant moments. Notice that the actuators usually distribute symmetrically on the mirror, the resultant forces of C_{i,M_x} and C_{i,M_y} are always 0, which means no extra resultant force will be introduced during the distribution of C_{i,M_x} and C_{i,M_y} . Figure 3 shows the force distribution of Algorithm 1.

Another algorithm firstly divides the actuators into m zones with one fixed point in each zone, then distributes each zone's fixed point's extra interaction force uniformly to the actuators in this zone. Assume the force adjustment of the i^{th} actuator in the j^{th} zone during the floatation support is $C_{i,j}$

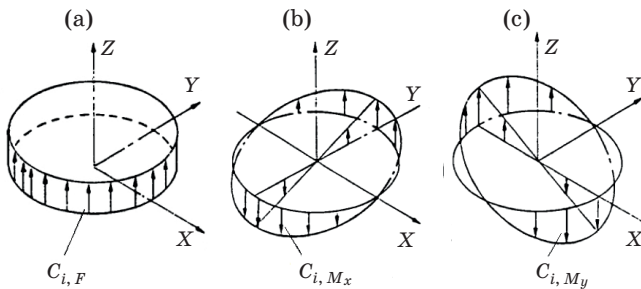


Fig. 3. Schematic of the force distribution in Algorithm 1. The (a) figure shows when compensating the resultant force, $C_{i,F}$ are uniformly distributed, the (b) and (c) figures show that when compensating the resultant moments, C_{i,M_x} and C_{i,M_y} are proportional to the lengths of the actuator's lever arms to the mirror's center.

($i = 1, 2, \dots, n/m, j = 1, 2, \dots, m$), it can be calculated as follows [13]:

Algorithm 2

$$C_{i,j} = -\frac{E_j}{n/m}, \quad (5)$$

$$i = 1, 2, \dots, n/m, j = 1, 2, \dots, m.$$

$C_{i,j}$ individually compensate the extra interaction force of the fixed point in each zone, as a result, the resultant force and moments of all the fixed points are also eliminated. The force distribution of Algorithm 2 is shown in Fig. 4.

The third algorithm [14] distributes C_i to compensate the fixed point's extra resultant force and moments respectively according to the force distribution of the actuators when the mirror is fitting piston and tilt/tip aberrations. Assume $F_{\text{piston}(i)}$ ($i = 1, 2, \dots, n$) to be the force of the i^{th} actuator when fitting a unit piston aberration with the mirror, and the resultant force is F_{piston} , so

$$F_{\text{piston}} = \sum_{i=1}^n F_{\text{piston}(i)}. \quad (6)$$

Similarly, assume $F_{x(i)}$ and $F_{y(i)}$ to be the forces of the i^{th} actuator when fitting a unit tilt and tip aberration with the mirror, and the resultant moment are respectively M_x and M_y , thus we have

$$\begin{aligned}
 M_x &= \sum_{i=1}^n (F_{x(i)} L_{x(i)}), \\
 M_y &= \sum_{i=1}^n (F_{y(i)} L_{y(i)}),
 \end{aligned} \quad (7)$$

where $L_{x(i)}$ and $L_{y(i)}$ are the lever arms of the actuators to the mirror center. Then C_i can be calculated as follows:

Algorithm 3

$$C_i = C_{i,F} + C_{i,M_x} + C_{i,M_y} =$$

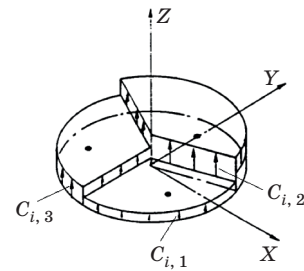


Fig. 4. Schematic of the force distribution in Algorithm 2. In this figure, the actuators are divided into 3 zones with 1 axial fixed point in each zone, the forces of the actuators in each zone are distributed uniformly when compensating the resultant force of the axial fixed point in their zone.

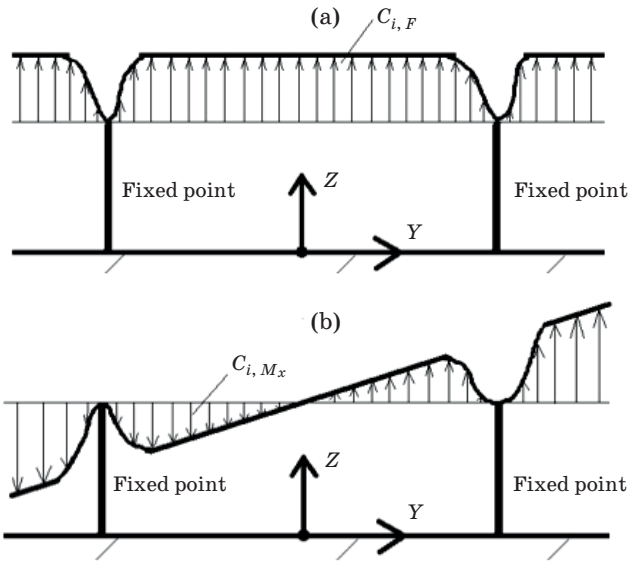


Fig. 5. Schematic of the force distribution of Algorithm 3 in a 2D case. The figures show when compensating the fixed point's resultant force and resultant moment on X axis, $C_{i,F}$ and C_{i,M_x} are respectively distributed according to the force distribution of the actuators when the mirror is fitting the piston and tip/tilt aberrations.

$$\begin{aligned}
 & -\sum_{j=1}^m E_j & -\sum_{j=1}^m (E_j L_{E_x(j)}) \\
 = & \frac{F_{\text{piston}(i)}}{F_{\text{piston}}} + \frac{F_{x(i)}}{M_x} & (8) \\
 & -\sum_{j=1}^m (E_j L_{E_y(j)}) \\
 + & \frac{F_{y(i)}}{M_y} \quad (i = 1, 2, \dots, n).
 \end{aligned}$$

Similar with Algorithm 1, $C_{i,F}$ is the fraction of C_i used to compensate the fixed point's resultant force, C_{i,M_x} and C_{i,M_y} are the fractions of C_i used to compensate the fixed point's resultant moments. The force distribution of Algorithm 3 in a 2-Dimension (2D) case is shown in Fig. 5.

3. A NEW FLOATATION SUPPORT ALGORITHM

All the algorithms above calculate the force adjustment of floatation support according to the feedback interaction forces of the fixed points. However, from Fig. 2 we can find that the "dents" on the mirror surface and the extra interaction forces of the fixed points always appear together, because actually the "dents" are caused by the extra forces, thus once floatation support can eliminate the "dents", the extra forces of the fixed points will also disappear. From this point, we propose a new floatation support algorithm based on the mirror surface's image detected by the S-H's sensor.

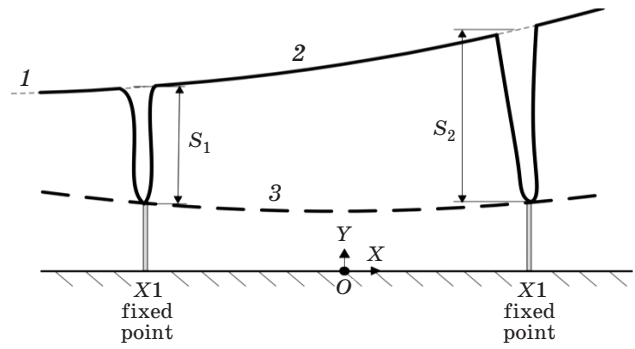


Fig. 6. Mirror surfaces before and after active correction without floatation support in a 2D case. 1 — Target mirror surface (M_1), 2 — actual mirror surface (M_2) when fitting M_1 , 3 — ideal mirror surface (M'_1).

A 2D case is shown in Fig. 6. After removing the tilt/tip, the target mirror surface of the S-H's sensor (or the ideal mirror surface in S-H sensor's view, shown as line 1 in Fig. 6) may be different with the real ideal mirror surface (shown as line 3 in Fig. 6), in fact, there are a piston and a tilt/tip between them. The consequence is that the actual mirror surface after the active correction (shown as line 2 in Fig. 6) deviates from the ideal position M'_1 , meanwhile, because the fixed points can't provide active forces and motions, M_2 can't perfectly overlap M_1 and has some "dents" at the positions of fixed points. M_2 corresponds to the Fig. 2b.

Notice that M'_1 differs from M_1 by just a piston and a tilt, assume a correction surface $M_{\text{correct}} = M'_1 - M_1 = a + lx$ which represent a curve consists of a piston and tilt, we have

$$a + l \begin{bmatrix} X_1 \\ X_2 \end{bmatrix} = - \begin{bmatrix} S_1 \\ S_2 \end{bmatrix}, \quad (9)$$

where X_1, X_2 are the coordinates of the two fixed points and S_1, S_2 are the deflections of the "dents" of M_2 at the two fixed points. The idea of the new algorithm is: if now we let the actuators add a set of forces which fit M_{correct} to the mirror, the actual result is the mirror surface is corrected from M_2 to M'_1 because of the limitation of the mirror's fixed points, thus the "dents" as well as the extra interaction forces of the fixed points will be eliminated. As a result, the force adjustment $C = [C_1, C_2, \dots, C_n]$ in the floatation support can be computed as follows:

Algorithm 4

$$C = (D^T D)^{-1} D^T M_{\text{correct}}. \quad (10)$$

Unlike the first 3 Algorithms, the 4th Algorithm doesn't utilize the feedback forces of the fixed points, instead, it directly makes use of the mirror surface's

image detected by the S-H's sensor. This simplified the hardware requirement of floatation support.

Notice that all the floatation support algorithms mentioned above introduce extern piston and tilt/tip to the primary mirror, these extern aberrations can be corrected by adjusting the secondary mirror of the telescope.

4. SIMULATION RESULTS OF THE ALGORITHMS

A 1.2 m thin primary mirror is used to simulate the performance of the floatation support algorithms mentioned in the previous sections. This mirror has a diameter of 1200 mm and a thickness of 50 mm, the radius-thickness ratio is 24. The material of the mirror is high borosilicate glass. Fig. 1 shows the configuration of the axial supports of the mirror. Shown in Fig. 1, the 33 axial actuators are divided into 3 zones A, B and C when implementing Algorithm 2. On the lateral side of the mirror there are 12 uniformly distributed lateral supports which can apply tangential support forces. In addition, there are 4 lateral fixed supports on the top, bottom, left and right of the mirror, which limit the 6 degrees of freedom of the mirror together with the 3 axial fixed points (Fig. 1).

We firstly adopt the mirror's gravitational deformations when it's mounted vertically to verify the performances of the algorithms. Shown in Fig. 2, when the mirror surface is corrected without floatation support, three "dents" appear on the residual surface at the positions of the fixed points and degrade the residual root mean square (RMS) to about 42 nm.

The results when applying the first 3 floatation support algorithms are shown in Fig. 7. It's clear that all the residual mirror surfaces after the correction have no "dents" at the fixed points, which means the extra interaction forces of the fixed points are eliminated. However, the 1st and 2nd algorithms are rather poor on maintaining the mirror surface, their force distribution methods aren't reasonable enough and introduce very large deformations, the residual RMS of the mirror surfaces after the floatation support with the first two algorithms are respectively 766 and 423 nm, which are even much larger than the one without floatation support (42 nm). The 3rd algorithm performs rather good, it introduces very little deformation and the residual RMS after the floatation support is only 3.3 nm.

For the 4th algorithm, in Fig. 2b corresponds to M_2 in Fig. 6, its deflections on the 3 fixed points are 80.4, 134 and -201 nm, and the coordinates of the 3 fixed points on X-Y plain are (0.5586, 0.1497 m), (-0.4089, 0.4089 m), (-0.1497, -0.5586 m), thus according to Eq. (9), the modification curve

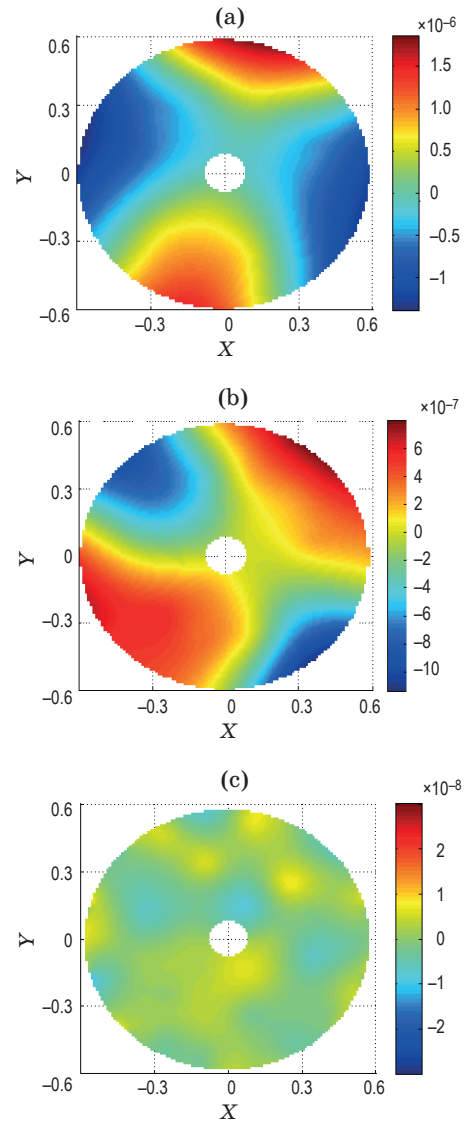


Fig. 7. Mirror surfaces after the active correction with the first 3 floatation support algorithms. (a) — 1st algorithm, RMS = 765.5 nm, (b) — 2nd algorithm, RMS = 423.4 nm, (c) — 3rd algorithm, RMS = 3.3 nm.

$M_{\text{correct}} = M'_1 - M_1 = a + l_x x + l_y y$ can be calculated as follows:

$$a + \begin{bmatrix} 0.5586 & 0.1497 \\ -0.4089 & 0.4089 \\ -0.1497 & -0.5586 \end{bmatrix} \begin{bmatrix} l_x \\ l_y \end{bmatrix} = - \begin{bmatrix} 8.04 \times 10^{-8} \\ 1.34 \times 10^{-7} \\ -2.01 \times 10^{-7} \end{bmatrix}. \quad (11)$$

Solving Eq. (11) we have $a = -4.5e-9$, $l_x = 4.0e-8$, $l_y = -3.6e-7$, substitute them into Eq. (10) and the force adjustment $C = [C_1, C_2, \dots, C_{33}]$ can be obtained. The final mirror surface after the floatation support with the 4th algorithm is shown in Fig. 8, the result shows this algorithm has a very good performance on maintaining the mirror surface during floatation support, the residual RMS is only 3.5 nm.

The performances of all the 4 algorithms on correcting the gravitational deformations of the 1.2 m mirror at other altitudes are also verified. The results are shown in Fig. 9.

Figure 9 shows similar results: the 1st and 2nd algorithms introduce very large deformations during the correction and their residual mirror surface RMS are very large, while the 3rd and 4th algorithm's performances are quite close and much better than

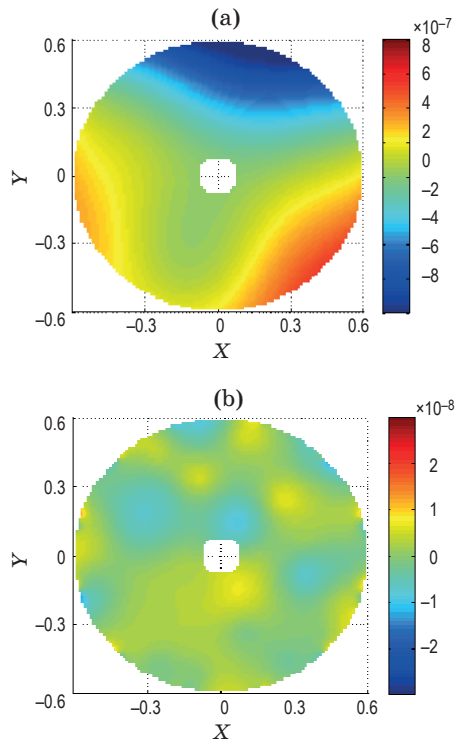


Fig. 8. Mirror surface after correction with the 4th floatation support algorithm.

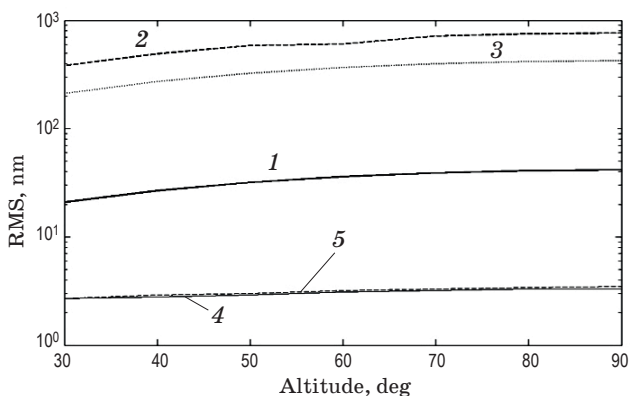


Fig. 9. Root mean square of the mirror surfaces after active correction with the 4 floatation support algorithms. 1 — no floatation support, 2 — result of the 1st floatation support algorithm, 3 — result of the 2nd floatation support algorithm, 4 — result of the 3rd floatation support algorithm, 5 — result of the 4th floatation support algorithm.

the first 2 algorithms, compared with the correction without floatation support, the residual RMS of the mirror surfaces of the 3rd and 4th algorithms are significantly reduced, the residual RMS of the mirror surfaces are only around 3 nm.

5. PERFORMANCE STUDY

As shown above, both the 3rd and 4th floatation support algorithms work excellently on correcting the thin mirror's surface. In order to conduct some deeper studies on these two algorithm's performances, we carry out some further researches.

5.1. Precision of the force sensor

The 3rd algorithm acquire the feedback interaction forces from the force sensors of the fixed points, as a result, the error of the force sensor may have some influences on the effect of this algorithm. We studied this error with the 1.2 m thin primary mirror via Monte-Carlo method, a Gaussian distributed force error is added here, the result is shown in Fig. 10. It shows the performance of the 3rd algorithm declines as the precision of the force sensor decreases, the average residual RMS of the corrected mirror surface increases to more than 9 nm when the standard deviation (RMS) of the force sensor's error reaches 20N. If we want the average residual RMS of the corrected mirror surface to be smaller than 4 nm, the precision of the force sensor has to be higher than 5N.

5.2. Precision of the Fixed Point's Position on the Mirror

The 3rd algorithm computes the extra moments with the feedback forces and the lever arms of the fixed points, while the 4th algorithm needs the fixed point's positions on the acquired image of the mirror surface to calculate $M_{correct}$, as a result, extra errors will be introduced if the positions of the fixed points on the mirror are not accurate because of the

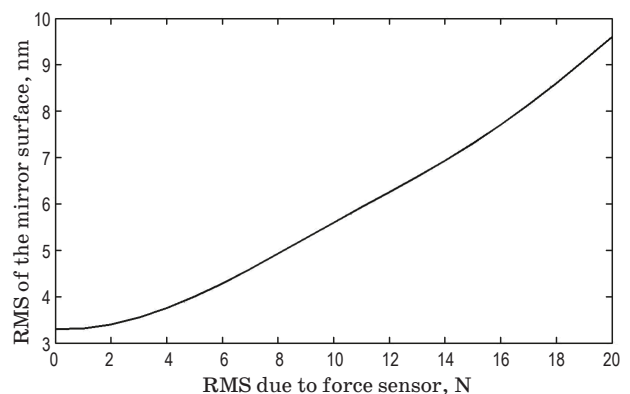


Fig. 10. Variation of the residual RMS of the mirror surface due to the error of the force sensor.

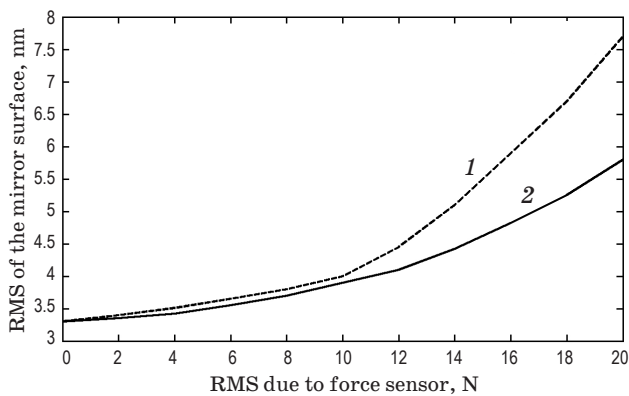


Fig. 11. Variation of the residual RMS of the mirror surface due to the error of the fixed point's position. 1 — algorithm 4, 2 — algorithm 3.

manufacture and alignment error. We conducted some researches on this error. The result is shown in Fig. 11.

Figure 11 shows the average residual RMS of the corrected mirror surfaces of both algorithms increase as the error of the fixed point's positions become larger — the mirror's average residual RMS reaches to nearly 8 and 6 nm for each algorithm when the RMS of the position errors are 20 mm. Meanwhile, although not very significantly, the 3rd algorithm shows better performance than algorithm 4th with this error. For both algorithms, the average residual RMS of the corrected mirror can be constrained to be lower than 4 nm when the position error is smaller than 10 mm.

5.3. Detection error of the S-H's sensor

Both the 3rd and 4th algorithms need the S-H's sensor to acquire the real-time mirror surface in order to calculate the correction forces, especially for the 4th algorithm — it needs the S-H's image to pick the deflections at the positions of the fixed points. Thus, we carried out some studies on the detection error of the S-H's sensor.

The result is shown in Fig. 12, the performances of both algorithms decrease as the S-H sensor's detection error increases, however, the residual mirror surface's RMS of the 4th algorithm increases faster than the 3rd algorithm, which means the effect of the 4th algorithm is much more sensitive and easier to be influenced by the S-H sensor's detection error. For the 1.2 m mirror, if we want to constrain the residual RMS of the mirror surface under 40 nm, the detection error of the S-H's sensor has to be less than 35 and 30 nm respectively for the 3rd and the 4th algorithm.

5.4. Comparison of the 3rd and 4th algorithms

Based on the studies in the previous sections, a brief comparison between the 3rd and the 4th floatation

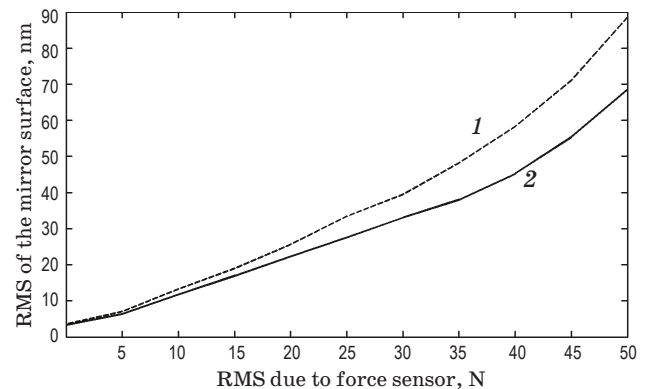


Fig. 12. Variation of the residual RMS of the mirror surface due to the S-H sensor's detection error. 1 — algorithm 3, 2 — algorithm 4.

Comparison of the 3rd and 4th algorithms

Algorithm	Algorithm 3	Algorithm 4
Residual mirror surface RMS, nm	Small (less 3.5)	Small (less 3.5)
Request of feedback force	Yes	No
Influenced by the feedback force error?	Yes	No
Influenced by the error of the fixed point's position on the mirror?	Yes (small)	Yes (large)
Influenced by the S-H sensor's detection error?	Yes (small)	Yes (large)

support algorithms are summarized. Table lists the details.

From Table we can find that both these two algorithms have very good performances during the floatation support, they introduce very little extra deformations and can correct the RMS of the mirror surface to less than 3.5 nm for the 1.2 m thin primary mirror. The 3rd algorithm which based on the feedback forces of the fixed points needs the force sensors to feedback the interaction forces and is easy to be influenced by the precision of the force sensors, while the 4th algorithm which based on mirror surface's image doesn't rely on the feedback forces but is easy to be influenced by the precision of the fixed point's positions on the mirror. Both algorithm's performances decline when the S-H sensor's detection error increases, but the 3rd algorithm is less sensitive and is more suitable for those situations with large detection noise. Compared with the 3rd algorithm, the 4th algorithm doesn't need the force sensors to feedback the interaction forces, thus it's more helpful to simplify the hardware requirement of floatation support.

6. CONCLUSION

This paper firstly introduces the function and influence of the thin mirror's axial fixed points in the mirror's active correction, then introduces the principle of floatation support as well as its 3 different force distribution algorithms. A new floatation support algorithm is proposed, it adjusts the actuators forces according to the mirror surface's image instead of the feedback interaction forces of the fixed points. Simulations are conducted on a 1.2 m primary thin mirror to verify these algorithm's performances, the results show that the new algorithm has as good performance as the best

traditional algorithm (the 3rd algorithm), the RMS of the 1.2 m mirror surfaces corrected by both the 3rd and the new algorithm are reduced to less than 3.5 nm after the floatation support. Comparisons are conducted between the 3rd and the new algorithms, it shows that the new algorithm are more sensitive to the fixed point's position deviation and the S-H's detection error, however, as it directly utilizes the S-H's image to adjust the actuator's forces, this new algorithm does not need the force sensors to feedback the interaction forces and is more helpful to simplify the hardware requirement of floatation support.

REFERENCES

1. Noethe L. Active optics in modern, large optical telescopes // Progress in Optics. 2002. V. 43. P. 3–69.
2. Cheng Jingquan. Principles of astronomical telescope design. Beijing: Chinese Science & Technology Press, 2003.
3. Kimbrell J.E., Greenwald D. AEOS 3.67 m telescope primary mirror active control system // Proc. SPIE. 1998. V. 3352. P. 400–411.
4. Martin H.M., Callahan S.P., Cuerden B. Active supports and force optimization for the MMT primary mirror // Proc. SPIE. 1998. V. 3352. P. 412–423.
5. Martin H.M., Cuerden B., Dettmann L.R. Active optics and force optimization for the first 8.4 m LBT mirror // Proc. SPIE. 2004. V. 5489. P. 826–837.
6. Gray P.M., Hill J.M., Davison W.B. Support of large borosilicate honeycomb mirrors // Proc. SPIE. 1994. V. 2199. P. 691–702.
7. Li Hongzhuang, Zhang Zhenduo. Active surface-profile correction of 620 mm thin-mirror based on floatation support // Acta Optica Sinica. 2013. V. 33. № 5. P. 0511001.
8. Schneermann M., Cui X., Enard D. ESO VLT III: The support system of the primary mirrors // Proc. SPIE. 1990. V. 1236. P. 920–928.
9. Sebring T.A., Dunham E., Millis R.L. The discovery channel telescope: A wide field telescope in northern Arizona // Proc. SPIE. 2004. V. 5489. P. 658–666.
10. Ashby D.S., Kern J., Hill J.M. The large binocular telescope primary mirror support control system description and current performance results // Proc. SPIE. 2008. V. 7018. P. 70184C.
11. Schipani P. Active optics primary mirror support system for the 2.6 m VST telescope // Appl. Opt. 2010. V. 49. № 8. P. 1234–1241.
12. Bennett R. Active mirror support using pneumatic actuators // Proc. SPIE. 2004. V. 5497. P. 91–102.
13. Miyawaki. Mirror support apparatus and system // Patent U.S. № 5115351. May 19, 1992.
14. Yao Ping, Zhang Xuejun, Zhang Yudong. Wind loading distortion analysis of an active primary mirror // Opto-Electron. Eng. 2011. V. 38. № 9. P. 71–76.